JOURNAL OF GEOPHYSICAL RESEARCH, VOL. 105, NO. D3, PAGES 4003–4018, FEBRUARY 16, 2000

# Trajectory hunting: A case study of rapid chlorine activation in December 1992 as seen by UARS

M. Y. Danilin,[1] M. L. Santee,[2] J. M. Rodriguez,[3] M. K. W. Ko,[1]
J. M. Mergenthaler,[4] J. B. Kumer,[4] A. Tabazadeh,[5] and N. J. Livesey[2]

**Abstract.** Trajectory hunting (i.e., a technique to find air parcels sampled at least twice over the course of a few days) is applied to analyze Upper Atmosphere Research Satellite (UARS) measurements in conjunction with the Atmospheric and Environmental Research, Inc. (AER) photochemical box model. As a case study, we investigate rapid chlorine activation in the Arctic lower stratosphere on December 29, 1992 associated with a polar stratospheric cloud (PSC) event. Eleven air parcels that have been sampled several times along 5-day trajectories at the 465 K (~46 hPa), 520 K (~31 hPa), and 585 K (~22 hPa) levels were investigated. For the first time, the latest versions of the Cryogenic Limb Array Etalon Spectrometer (CLAES, version 9) and Microwave Limb Sounder (MLS, version 5) data sets are analyzed, and their consistency is assessed. A detailed sensitivity study with the AER photochemical box model along these trajectories leads to the conclusion that for the December 24-29, 1992 episode (1) the individual CLAES version 9 $ClONO_2$ and MLS version 5 ClO measurements are self-consistent within their uncertainties; and (2) most of the time, UARS measurements of ClO, $ClONO_2$, $HNO_3$, and aerosol extinction at 780 $cm^{-1}$ agree within the range of their uncertainties with the model calculations. It appears that the $HNO_3$ and aerosol extinction measurements for four parcels at 520 K look more supportive for the nitric acid trihydrate (NAT) scheme. However, the uncertainties in the individual UARS measurements and U.K. Meteorological Office temperature do not allow a definite discrimination between the NAT and supercooled ternary solution (STS) PSC schemes for this chlorine activation episode in December 1992.

## 1. Introduction

To understand the current and predict the future ozone depletion in the polar regions, it is necessary to separate the effects due to dynamical and chemical processes. One effective strategy for achieving this goal is to identify air parcels that have been sampled twice or more over the course of a few days. The difference between the initial and final concentrations of ozone (or any other species) for these parcels can then be attributed solely to chemical processing since dynamical effects are eliminated.

"Trajectory hunting" is a technique to find air parcels that have been sampled at least twice over a period of several days. The trajectory hunting approach that we employ in this paper is similar to the Match technique [e.g., *Rex et al.*, 1998]. However, there are clear differences. For example, so far the Match technique is associated only with analysis of the ozone loss rate along matched trajectories within a 10-day interval between initial and final points [*von der Gathen et al.*, 1995; *Rex et al.*, 1997, 1998]. Thus the Match approach searches for a rather small signal and requires good statistics to make a robust conclusion. On the other hand, the Match technique has the advantage of dealing with ozonesonde measurements, which are more precise and also have much better vertical and horizontal resolution than the satellite data. This technique can also be applied to measurements obtained by different platforms. For example, *Pierce et al.* [1997] compared trajectory-matched observations from the UARS Halogen Occultation Experiment (HALOE) with aircraft ER-2 measurements. *Bacmeister et al.* [1999] applied trajectory mapping to a comparison of long-lived tracer data obtained by the ER-2 and Cryogenic Infrared Spectrometers and Telescopes for the Atmo-

[1]Atmospheric and Environmental Research, Inc., Cambridge, Massachusetts.
[2]Jet Propulsion Laboratory, Pasadena, California.
[3]Department of Marine and Atmospheric Chemistry, University of Miami, Miami, Florida.
[4]Lockheed Martin Palo Alto Research Laboratory, Palo Alto, California.
[5]NASA Ames Research Center, Moffett Field, California.



Paper number 1999JD901054.
0148-0227/00/1999JD901054$09.00

sphere (CRISTA) in November 1994. Recently, *Steele et al.* [1999] investigated the evolution of polar stratospheric clouds (PSCs) during Antarctic winter using Polar Ozone and Aerosol Measurement (POAM) II data and a microphysical model.

Analysis of short-lived species along parcel trajectories requires a photochemical model. Utilization of Upper Atmosphere Research Satellite (UARS) Cryogenic Limb Array Etalon Spectrometer (CLAES) and Microwave Limb Sounder (MLS) data combined with a photochemical box model is particularly promising for the trajectory hunting technique because of the relatively large number of measured species ($O_3$, $HNO_3$, ClO, $ClONO_2$, $N_2O$, $CH_4$, $H_2O$, and aerosol extinction coefficient) and frequent sampling (~1300 profiles per day). Use of "matched" trajectories better constrains the model, providing initial and final concentrations together with necessary parameters along the trajectories. Data from multiple instruments complement each other and provide additional constraints on the model calculations. Also, the use of satellite data affords coverage over a much larger horizontal and vertical area than can be achieved with balloon or aircraft measurements. In this context the trajectory hunting technique could be useful for validation studies of new satellite platforms and instruments.

The goals of this study are (1) to perform a case study applying the trajectory hunting technique in which concentrations and aerosol parameters calculated by the AER box model (representing photochemical and PSC processes) are compared with UARS measurements for air parcels sampled multiple times during a 5-day period encompassing a chlorine activation event, (2) to determine whether the trajectory hunting approach can be applied to infer information about PSC phase and/or composition by comparing the measurements with model predictions for different PSC schemes, and (3) to investigate the consistency between the new version 9 CLAES and version 5 MLS data sets in the context of this activation episode.

The structure of this paper is the following: Section 2 briefly describes the MLS and CLAES instruments and provides some specific information about the species utilized in this study. Section 3 describes in detail the selection of the trajectories and the data analysis. Section 4 discusses the AER model initialization, while section 5 presents results of the model calculations and discussion. Section 6 summarizes the main findings of this study.

## 2. Data and Instrument Descriptions

### 2.1. MLS

MLS has been acquiring millimeter-wavelength emission measurements of the stratosphere in both hemispheres since late September 1991. The microwave limb sounding technique and the MLS instrument are described in detail by *Waters* [1993] and *Barath et al.* [1993], respectively. Validation of the MLS instrument calibration and the primary MLS measurements is described for version 3 (v.3) data in a special issue of *Journal of Geophysical Research* (*101*(D6), 9539–10,476) dedicated to the evaluation of the UARS data. In particular, *Waters et al.* [1996] report in detail on the validation of the v.3 MLS ClO data. UARS MLS observations of lower stratospheric ClO have been presented previously for several northern and southern hemisphere winters [*Waters et al.*, 1993, 1995; *Manney et al.*, 1996a; *Santee et al.*, 1996, 1997]; in addition, *Santee et al.* [1996] discuss some of the differences in Arctic ClO between v.3 and v.4 data.

In this paper we use results from new v.5 MLS retrieval algorithms. The v.5 data will constitute the final archived MLS data set. Here we describe only briefly the pertinent findings from preliminary validation studies; a detailed assessment of the quality of the various MLS v.5 geophysical data products will be given elsewhere [*N. Livesey et al.*, manuscript in preparation]. The sequential estimation method used in previous versions of the data processing has been replaced by a matrix-based optimal estimation approach, permitting the use of a more complete error budget calculation [*N. Livesey et al.*, manuscript in preparation]. Altogether, the various refinements in the forward model and retrieval algorithm have led to much better fits to the radiometric data. In addition, in the v.5 data set geophysical parameters are reported at twice the vertical resolution of previous MLS data sets (6 surfaces per decade in pressure, as opposed to 3). In actuality, effects such as smearing by the instrumental field of view and radiance noise will reduce the true resolution. In particular, for the ClO measurements, which have a lower signal-to-noise ratio than other MLS species, the information content of the data is closer to 4-5 surfaces per decade in pressure rather than 6; that is, the true vertical resolution of the v.5 ClO is not quite twice that of the previous versions.

In v.5 retrieved vortex, ClO is spread over a larger vertical range than before, broadening the peak and reducing peak mixing ratios. In general, the peak in the retrieved profile has moved up from 46 hPa in v.4 to 32 hPa (which was not formerly a retrieval surface) in v.5. In addition, a small negative bias (0.1-0.2 ppbv at 4.6 to 46 hPa) that was present in average nighttime ClO values in previous data versions has been eliminated, and the unrealistic behavior of ClO with respect to solar zenith angle at 100 hPa has been corrected [see *Waters et al.*, 1996]. For an individual v.5 ClO profile the estimated noise uncertainty, which represents the precision of the measurement, is ~0.4 ppbv in the lower stratosphere; this uncertainty can be reduced by averaging over several profiles. In addition, the bias and scaling uncertainties in the v.5 ClO data are estimated to be 0.1 ppbv and 7.5%, respectively (see *Waters et al.* [1996] for further information on these uncertainties). All three uncertainties (noise, bias, and scaling)

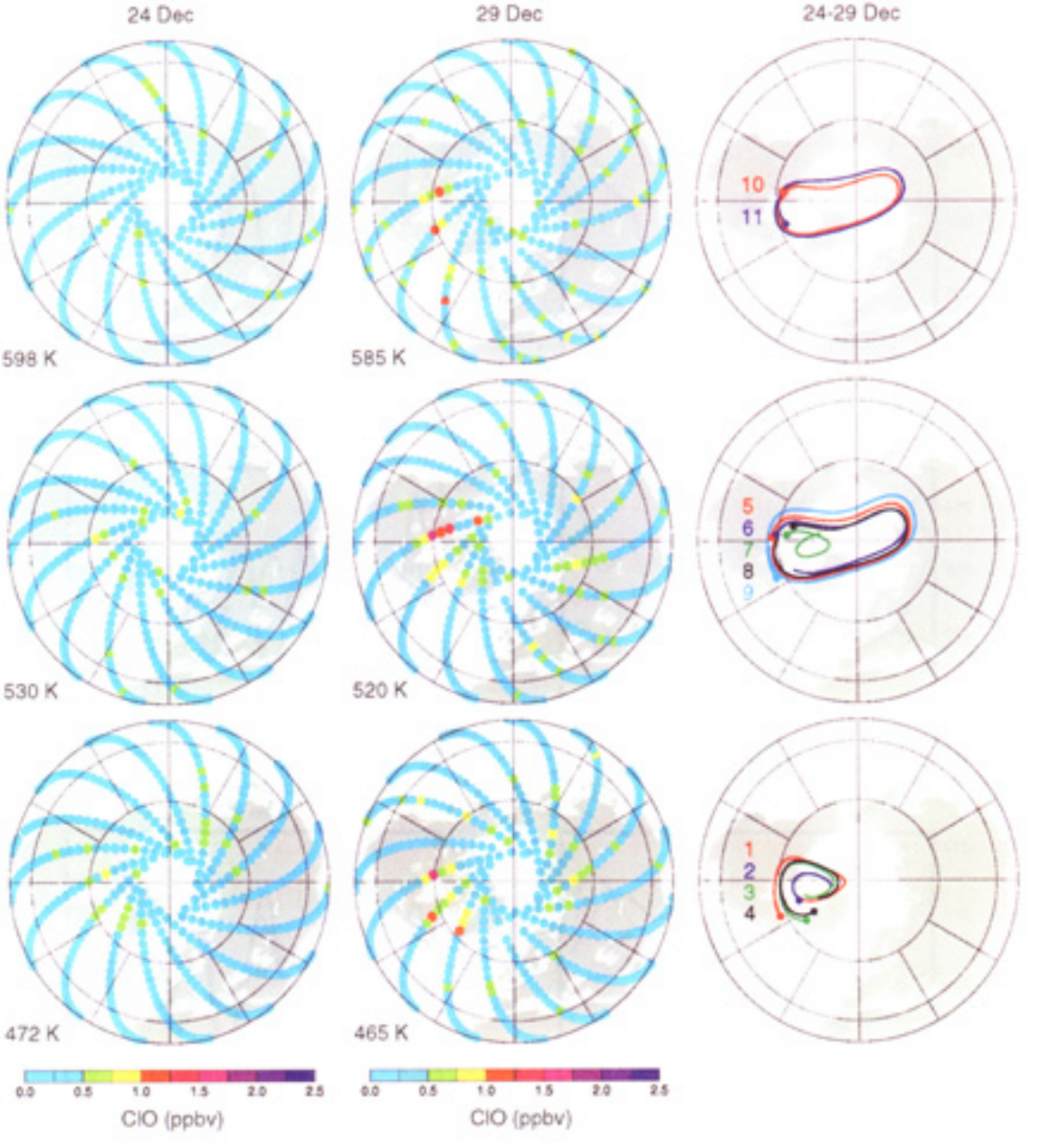


**Plate 1.** MLS v.5 ClO measurements at 598-585 K (top row), 530-520 K (middle row), and 472-465 K (bottom row) on December 24 (left column) and December 29, 1992 (middle column). Trajectories followed by individual air parcels during this 5-day period are shown for each level in the right column. Thick dots show the parcel positions on December 29. These 11 parcels satisfy the match criteria (see text) and are used for the model analysis.

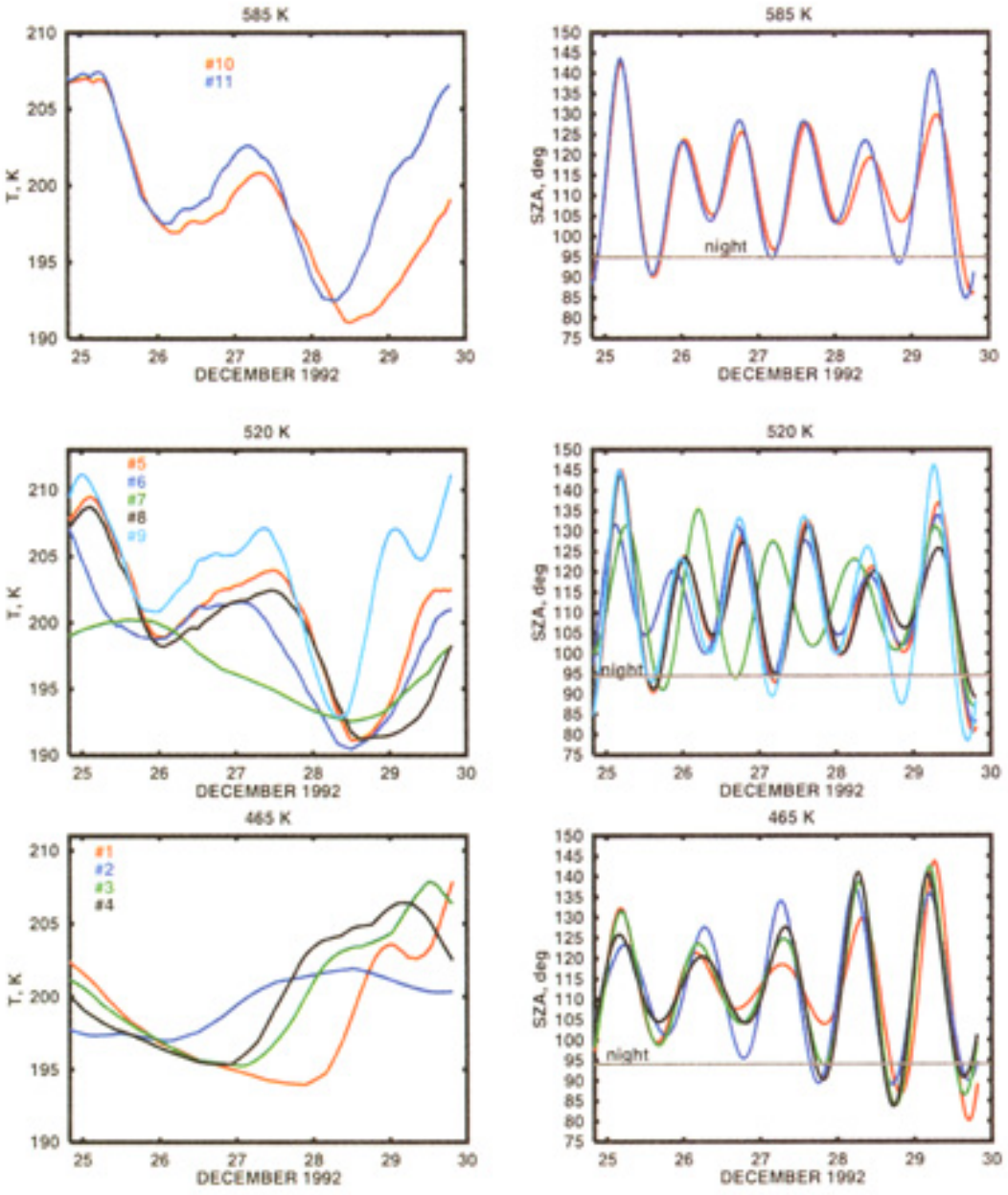


**Plate 2.** Evolution of temperature (left column) and SZA (right column) along the trajectories shown in Plate 1. The trajectories in Plate 1 and temperature and SZA in Plate 2 are shown by the same colors.

are root-sum-squared to derive the error bars shown on the data points in section 5.

MLS lower stratospheric $O_3$ data, which are used for model initialization (see section 4), are significantly improved in v.5. Preliminary evaluation of the quality of the $O_3$ data (from the 205 GHz radiometer) yields an estimate of about 0.4 ppmv for the combined error (including accuracy and precision terms) of an individual profile in the lower stratosphere.

Although CLAES $HNO_3$ is used for model initialization, MLS $HNO_3$ data are also compared to model results in section 5. A thorough analysis of 6 years of MLS v.4 $HNO_3$ data was presented by *Santee et al.* [1999]. This study included an intercomparison of MLS and CLAES $HNO_3$ data over the entire lifetime of the CLAES instrument that showed excellent agreement in the overall morphology of and timing of the changes in the $HNO_3$ distribution measured by the two instruments. The MLS $HNO_3$ retrievals are also significantly improved in v.5, with the noise uncertainty of an individual profile ranging between 1.0 and 1.8 ppbv throughout the lower stratosphere. Although the estimated accuracy has not yet been quantified because a sufficient number of comparisons with correlative data sets have not been made, preliminary indications are that MLS $HNO_3$ mixing ratios exceed those of correlative data by ~40% over the domain 68 to 15 hPa inside the vortex when $HNO_3$ is enhanced. Thus differences between the MLS and CLAES $HNO_3$ fields can exceed 5 ppbv for typical $HNO_3$ values in the stratosphere. Although the v.5 MLS data overestimate winter polar $HNO_3$ abundances (in the nondenitrified areas) by several ppbv, since in this paper we will be most concerned with relative variations, these systematic errors are of less importance. The quality control measures outlined by *Santee et al.* [1998] were applied to the v.5 data in this study; for example, retrievals that were strongly influenced by the a priori estimate were discarded.

It can be shown [*Waters*, 1993] that, for optically thin situations, the relative contribution to the measured limb emission (the weighting function) along the observation path has a Gaussian distribution, the width of which sets the MLS horizontal resolution along the line of sight to ~400 km. The UARS orbital motion during the time of a limb scan smears the measurement over ~400 km in a direction perpendicular to the MLS line of sight. Thus the retrieved MLS values at a particular geographic location and atmospheric level essentially represent averages over approximately a $400\times400\times3$ km$^3$ volume of air. It must be borne in mind that an assumption inherent in using satellite data for trajectory hunting studies is that the composition of the atmosphere is uniform over the instrument field of view.

### 2.2. CLAES

CLAES measures infrared thermal emission in nine spectral regions between 3.5 $\mu$m and 13 $\mu$m [*Roche et al.*, 1993]. CLAES has vertical and horizontal resolutions of about 3 km and 400 km × 400 km, respectively. MLS and CLAES observations are essentially simultaneous and co-located (typically to within a few tens of kilometers). For this study we utilize CLAES measurements of $N_2O$, $CH_4$, $ClONO_2$, $HNO_3$, and aerosol extinction coefficients from the 780 cm$^{-1}$ (or 12.82 $\mu$m) channel. Validation of each of these species is described for version 7 (v.7) data in a series of papers in the special issue of JGR [*101*(D6), 1996]. Further descriptions of CLAES versions 7, 8, and 9 can be found with these data on the Distributed Active Archive Center (DAAC) at the NASA Goddard Space Flight Center (GSFC).

In this paper we present results from new v.9 CLAES retrieval algorithms. CLAES v.9 $ClONO_2$, $HNO_3$, $N_2O$, and aerosol extinction from the 780 cm$^{-1}$ channel were not changed appreciably from the two previous versions since the v.9 software upgrades were not directed to these particular constituents. However, there were small changes in the vertical registration and the temperature retrieval that affected all species. Relative to the more intensely validated v.7 product, the volume mixing ratio of $ClONO_2$ in v.9 agrees slightly better with correlative data. For example, the average difference between CLAES $ClONO_2$ profiles and the suite of corresponding correlative profile measurements used in the v.7 $ClONO_2$ validation paper [*Mergenthaler et al.*, 1996] is smaller for v.9 data in the 19-21 km region (about 3% in v.9 versus 5% in v.7). In the northern high latitudes the $ClONO_2$ distribution is raised in altitude by about 1 km on average and is increased in magnitude by about 10%. $HNO_3$ is similarly changed. Like $ClONO_2$, the v.9 $k_{abs}(780)$ profile is registered about 1 km higher in altitude than the v.7 profile. Nitrous oxide is measured by CLAES using the 1257 cm$^{-1}$ channel. Our estimate of an upper bound for precision of individual v.9 $N_2O$ profiles in the lower stratosphere is 5-7% under midlatitude summer conditions and about 35% in the polar winters. While a portion of this estimate comes from unfiltered atmospheric variability, the CLAES retrieval is expected to be less precise in polar regions during winter when strong horizontal gradients in temperature and species are expected. Our preliminary analysis shows that v.9 $N_2O$ measurements are within ±5% of the available correlative comparisons below 30 km, an improvement over v.7 which was within +5 to +15% of the correlative data [*Roche et al.*, 1996].

Precisions with v.9 appear to be similar to earlier versions for the species involved in this study. Our estimate of the total uncertainty of an individual $ClONO_2$ measurement is about 20%. As in v.7, $HNO_3$ accuracy and precision are estimated to be about 15% and 0.3-1.0 ppbv from 70-3 hPa, respectively. The total uncertainty of the surface area density (SAD) values derived from the CLAES 780 cm$^{-1}$ measurements (see Section 4 below) is about 40% based on the assumptions that (1) the uncertainty of an individual CLAES 780 cm$^{-1}$ measurement is about 20%, (2) the conversion between aerosol extinction coefficient and SAD in-

troduces an additional uncertainty of about 30% (S. T. Massie, *personal communication*, 1999), and (3) these errors are independent. Detailed validation of the v.9 CLAES products is in preparation and will be described elsewhere.

## 3. Selection of Trajectories and Data Analysis

We examine an episode of rapid chlorine activation associated with PSC activity in the Arctic polar region. We concentrated on events for which both MLS and CLAES measurements are available and the evidence of chlorine activation is unambiguous, that is, high ClO values in regions of low temperature where ClO was not enhanced a few days earlier. Since CLAES data are available from October 1991 to May 1993, only two Arctic winters could be analyzed. Between these two winters we picked the most pronounced episode of rapid chlorine activation in December 1992 for our case study. This chlorine activation episode is illustrated in Plate 1, which shows MLS ClO data for both December 24 and 29, 1992. Only data from the "day" side of the orbit are shown because ClO abundances drop sharply in regions where the solar zenith angle is greater than 94°, due to reduction of the ClO production of ClO via photolysis of $Cl_2O_2$ and $Cl_2$. The ClO mixing ratios are represented at the actual MLS measurement locations (i.e., no horizontal binning or averaging has been performed). The MLS data have been vertically interpolated onto constant potential temperature ($\Theta$) surfaces at 585 K (corresponding to ~24 km or ~22 hPa for the low temperatures characteristic of the polar vortex), 520 K (~21 km or ~31 hPa), and 465 K (~19 km or ~46 hPa) using United Kingdom Meteorological Office (UKMO) temperatures [*Swinbank and O'Neill*, 1994]. As evident in Plate 1, MLS detected a rapid increase in ClO of ~0.5-1.0 ppbv between December 24 and 29 above northern Canada and Greenland on all three $\Theta$ surfaces.

On each $\Theta$ level, 600 equally spaced parcels were initialized in a 20° × 60° latitude/longitude box encompassing all the enhanced ClO points on December 29, and 5-day back trajectories were calculated. As described in more detail by *Manney et al.* [1994], the three-dimensional trajectory calculations use horizontal winds and temperatures from the UKMO data assimilation. To account for diabatic effects, a recent version of the middle atmosphere radiation code MIDRAD [*Shine*, 1987] is used to compute vertical velocities $(d\theta/dt)$. Although the large-scale air motion is generally simulated well by these calculations, *Manney et al.* [1995] found that they slightly overestimated the magnitude of the diabatic descent in the midstratosphere in the 1992-1993 Arctic early winter, based on comparisons with passive tracers measured by CLAES on UARS. For comparison purposes, and to effectively bound the problem, we have also calculated the 5-day back trajectories using an isentropic version of the model, whereby the potential temperature of the parcels is held constant along the trajectories. Note that the trajectory hunting technique should only be used for simulations shorter than ~10 days because of the larger accumulated uncertainties in trajectory calculations done for longer periods [e.g., *Schoeberl and Sparling*, 1995; *Morris et al.*, 1995].

From the original set of parcels described above, we identified candidate parcels that were nearly coincident in space and time (within 2° in latitude, 200 km in longitude, and 2 hours in time) with enhanced ClO points on December 29 and with any MLS measurement points 5 days earlier on December 24. In addition to this proximity requirement, we imposed the further constraint that both the initial and final locations of the parcels had to be inside the boundary of the polar vortex (as defined by the region of strong gradients in the UKMO potential vorticity (PV) field). Parcels satisfying these criteria were still rejected if their solar zenith angles at the trajectory endpoint on December 29 exceeded 95° (in which case the model could not reproduce the enhanced ClO values, see below) or their initial ClO values at the trajectory on December 24 exceeded 0.5 ppbv (in which case some degree of prior chlorine activation was indicated). The number of "matches" depended on the number of individual enhanced ClO points, the number of parcels initialized in the original box, the meteorological conditions, and the "match" criteria. Many matches were duplicative in the sense that several parcels may have started off near the same high-ClO point, followed similar paths, and thus also ended up nearest the same point at the termination of the back trajectory calculation. Our goal in selecting the final subset of parcels for which model runs were performed was to represent the widest range of trajectory behavior possible. After taking into account all of these considerations, we selected four parcels ending at 465 K (parcels 1, 2, 3, and 4), five parcels ending at 520 K (parcels 5, 6, 7, 8, and 9), and two parcels ending at 585 K (parcels 10 and 11).

The paths followed by the selected parcels during the 5-day interval between December 24 and 29 are illustrated in Plate 1. Thick dots denote the parcel positions on December 29. Overall diabatic effects over the course of the 5 days were found to be essentially similar for all parcels initialized on a given $\Theta$ surface, with parcels exhibiting descent of approximately 7 K, 10 K, and 13 K to end up at 465 K, 520 K, and 585 K, respectively, on December 29. Thus the MLS data for December 24 are shown at 472 K, 530 K, and 598 K, while the data for December 29 are shown at 465 K, 520 K, and 585 K. However, for simplicity, we refer to the three levels as "465 K", "520 K", and "585 K" throughout the paper. Large changes in potential vorticity along a trajectory are indicative of substantial influence from diabatic effects or small-scale diffusion [e.g., *Rex et al.*, 1998]. To guard against these situations, we checked

the PV history (derived from the UKMO analyses) of each of the selected parcels and found that they all exhibit nearly constant values of PV relative to the vortex edge (not shown) throughout the 5-day trajectory run. In addition, these particular parcels follow paths that are confined well inside the vortex. Since these parcels do not traverse regions of strong tracer gradients, it is unlikely that the trace gas concentrations at their locations are altered significantly by any horizontal mixing that may occur.

In the trajectory calculations the parcel positions are saved every half hour. For comparison with the box model results, we require an estimate of the measured quantities at points along the trajectories. This is accomplished in a multi-step process at each time step. First, the data are vertically interpolated onto the parcel $\Theta$ surface at that time step. Next a gridding procedure is applied, whereby a weighted average is taken of all observations falling within a prescribed distance in latitude, longitude, and time of the parcel position. In this procedure all data points contributing to the average are weighted by their distance (in space or time) from the parcel location. Various combinations of weighting parameters were tested. The gridding is not especially sensitive to the particular weighting function used; here we employed a $\cos^2$ function, but a Gaussian function produced similar results. The half-width values are 2° in latitude, 7° in longitude, and 0.1 days in time, and only data within one half-width of the parcel position are included. These half-widths are deliberately chosen to be very tight so that at most one or two data points go into the average unless the data are very closely spaced (as occurs near the orbit turnaround point near the pole; see Plate 1); this is done to minimize the effects of smoothing while still permitting more than one data point recorded close to a parcel's position to influence the estimate of the measured value at that point. If no measurements fall within the allowable distance, then the gridding routine returns a bad data value. As described above, the particular parcels used here were selected to have MLS ClO measurements within the prescribed distance at both the initial and final time steps, but because of the timing of the measurements, the orbit track spacing, and the along-track resolution, data estimates are unavailable for many of the other time steps along the trajectory. Furthermore, because the trajectory time step is much smaller than the time half-width employed in the gridding procedure, the gridded data tend to become available in short clumps along the trajectory (see section 5).

The evolution of the temperature and the solar zenith angle (SZA) along the selected trajectories is shown in Plate 2 for all three $\Theta$ surfaces. The temperature histories were constructed by interpolating UKMO temperatures (available on a uniform grid once daily, at 1200 UT) to the time, latitude, longitude, and $\Theta$ values of the parcels at each time step throughout the 5-day run. For most of the parcels, temperatures dipped to near or below the NAT threshold (i.e., about 196, 194, and 192 K at 465, 520, and 585 K, respectively) during the 2 days preceding the MLS observation of high ClO, suggesting that PSC processing converted chlorine into $Cl_2$ and $Cl_2O_2$, which were photolyzed to ClO at the final points (if SZA$\leq$95°).

## 4. Model Initialization

The AER photochemical box model [*Danilin et al.*, 1998] with a comprehensive set of photolytic, gas-phase, and heterogeneous reactions and their recommended kinetic data [*DeMore et al.*, 1997] is used. Table 1 lists the heterogeneous reactions included in the model. Our model has an option to use either nitric acid trihydrate (NAT) or supercooled ternary solution (STS) PSC schemes. For the NAT scheme, PSC particles are formed independently of the sulfate aerosol when the $HNO_3$ vapor pressure exceeds the NAT threshold according to *Hanson and Mauersberger* [1988]. The NAT SAD is calculated assuming no supersaturation and a particle diameter of 1 $\mu$m with a density of 1.62 g/cm$^3$. In the STS scheme, additional uptake of $HNO_3$ and $H_2O$ onto ambient sulfate aerosol is calculated below 205 K according to *Tabazadeh et al.* [1994]. This scheme keeps the particle concentration constant, and the increase in STS SAD is calculated based on the additional amount of $HNO_3$ and $H_2O$ condensed and the size distribution of ambient sulfate aerosol (see below).

The model is initialized using MLS v.5 $O_3$ (profiles and partial column above 100 hPa), prototype nonlinear retrievals of MLS $H_2O$ [*Pumphrey*, 1999], and CLAES v.9 $ClONO_2$, $HNO_3$, $N_2O$, and $CH_4$ on December 24. Total inorganic chlorine $Cl_y$ is defined from the $Cl_y$-$N_2O$ correlation according to *Woodbridge et al.* [1995] using CLAES measurements of $N_2O$ at the initial points. This approach gives 2.4-2.7 ppbv, 2.6-2.8 ppbv, and ~2.9 ppbv of $Cl_y$ along trajectories at 465, 520, and 585 K, respectively. Possible errors in $Cl_y$ do not affect our conclusions because $ClONO_2$ is a limiting factor for chlorine activation during the episode considered (see discussion in Section 5). The lack of simultaneous measurements of all chlorine species leads to uncertainties in the partitioning of the initial $Cl_y$. For all trajectories, ClO is initialized to $ClO^{MLS}$. Initial $Cl_2O_2$ is calculated using a steady state assumption from the $ClO^{MLS}$ as $Cl_2O_2 = k_f(ClO^{MLS})^2/(J_{Cl_2O_2} + k_d)$, where $k_f$ and $k_d$ are the rate constants of the $Cl_2O_2$ formation and thermal decomposition reactions, respectively, and $J_{Cl_2O_2}$ is the photolysis rate of $Cl_2O_2$. Since no HALOE HCl measurements are available for the points of interest because HALOE did not measure poleward of 50°N in December 1992, initial HCl is set to $Cl_y - ClONO_2^{CLAES} - ClO^{MLS} - 2Cl_2O_2$. Total inorganic bromine $Br_y$ is defined according to *Wamsley et al.* [1998] and is about 18-20 part per trillion by volume (pptv) at these levels

**Table 1.** Heterogeneous Reactions on Sulfate Aerosol and PSCs Included in the Model

| | Reaction | | |
|---|---|---|---|
| (R1) | $N_2O_5 + H_2O$ | $\longrightarrow$ | $HNO_3 + HNO_3$ |
| (R2) | $BrONO_2 + H_2O$ | $\longrightarrow$ | $HOBr + HNO_3$ |
| (R3) | $ClONO_2 + H_2O$ | $\longrightarrow$ | $HOCl + HNO_3$ |
| (R4) | $ClONO_2 + HCl$ | $\longrightarrow$ | $Cl_2 + HNO_3$ |
| (R5) | $HOCl + HCl$ | $\longrightarrow$ | $Cl_2 + H_2O$ |
| (R6) | $HOBr + HCl$ | $\longrightarrow$ | $BrCl + H_2O$ |

with initial BrO=$BrONO_2$=$Br_y/2$. Since no reliable $NO_x$ (= NO+$NO_2$) measurements are available for the points considered, we set $NO_x$ to 0.2 ppbv (based on aircraft measurements [*Kawa et al.*, 1992]) and assume that initial NO=$NO_2$=$NO_x/2$. Sensitivity studies with different $NO_x$ concentrations are also performed (see section 5). Total reactive nitrogen $NO_y$ is taken to be $HNO_3^{CLAES}$ + $ClONO_2^{CLAES}$ + $NO_x$ + $BrONO_2$ and is about 11-12 ppbv at 465 K and 13-15 ppbv at 520 and 585 K. The amounts of $Cl_y$, $Br_y$, and $NO_y$ for each parcel are kept constant during the model runs. This assumption is well-justified since the possibility of denitrification or dehydration in the parcels considered can be ruled out because the minimum temperature attained along their trajectories is 7-8 K above the ice frost point and stays below the NAT threshold too briefly (up to 1-2 days) to cause denitrification (*A. Tabazadeh et al.*, manuscript in preparation).

Sulfate aerosol SAD is initialized using the CLAES aerosol extinction measurements at 780 $cm^{-1}$ according to *Massie et al.* [1998]:

$$SAD = C \times \exp(12.77 + 1.681 \times B + 0.04614 \times (B)^2), \quad (1)$$

where $C$ is the scaling factor (= 0.66, 0.67, and 0.47 $\mu m^2/cm^3$ at 465, 520, and 585 K, respectively), $B$= $\ln(k_{abs}(780))$ and $k_{abs}(780)$ is the aerosol absorption (in $km^{-1}$) measured by CLAES in the 780 $cm^{-1}$ channel. We use the coefficients for binary sulfate aerosol in equation (1) from *Massie et al.* [1998] since initial temperature (about 200-210 K) on December 24 is too warm to account for additional $HNO_3$ uptake. We assume that ambient aerosol particles have radius of 0.3 $\mu$m.

## 5. Results of Trajectory Calculations and Discussion

We performed model runs for each parcel shown in Plate 1. Comparisons of the model calculations with UARS data are shown in Figures 1-3 for ClO, $ClONO_2$, $HNO_3$, and SAD for all parcels except parcel 6 at 520 K. Results for parcel 6 are not shown since they are very similar to those for parcel 5, as could be anticipated from Plates 1 and 2. Comparison of model results and MLS measurements for ozone will be shown in Plate 3 only since the model calculates almost constant mixing ratios of $O_3$ due to the lack of sunlight along the selected trajectories, making its temporal evolution uninteresting for showing in Figures 1-3.

As mentioned in the previous section, there are uncertainties in the model initialization despite the use of available UARS measurements. We define our baseline case scenarios as those when initial $ClONO_2$, ClO, and SAD are equal to their measurements from UARS, initial $NO_x$ is equal to 0.2 ppbv, and temperature along the trajectories is equal to that from the UKMO analyses. The baseline scenarios are run for both PSC schemes at all three levels and are shown by the dashed and dotted lines in Figures 1-3 for the STS and NAT PSC schemes, respectively. For the NAT scheme the sum of NAT and ambient sulfate aerosol SADs are shown. The CLAES aerosol extinction measurements at 780 $cm^{-1}$ converted to SAD using equation (1) are shown with 40% error bars in these figures.

Additionally, we performed sensitivity runs in which the following parameters are changed: (1) temperature is lowered by up to 2 K uniformly along the trajectories; (2) initial SAD and $ClONO_2$ are reduced or increased within the range of their uncertainties; and (3) initial $NO_x$ is varied within the range 0.1-0.3 ppbv. The reason to decrease the UKMO temperature is that *Manney et al.* [1996b] showed that, compared to radiosondes, UKMO temperatures have a systematic warm bias of ~1-3 K during most of the northern winter. Among our numerous sensitivity runs we show results only for the "fit" scenarios, which are intended to provide better agreement with measurements on December 29. These fit scenarios use the STS scheme and the modifications of the baseline scenario shown in Table 2 for each individual parcel. These fit scenarios are shown by solid lines in Figures 1-3 and provide better agreement between model calculations and UARS measurements. However, they are not unique. Changes in different parameters in the model may produce similar response in ClO; for example, increasing SAD, decreasing initial $NO_x$, using colder temperature or some combination of these parameters produce increase in ClO. Also, the NAT scheme with slightly different modified temperature, initial $ClONO_2$, SAD, and $NO_x$ could produce similar results to those shown in Figures 1-3 for the STS fit scenarios. The goal of the fit model calculations is to show that better agreement with UARS measurements can be obtained within the range of the uncertainties of the model initialization and UKMO temperature. These fit scenarios are not a test of overall data quality and should be considered as a tool to understand whether model calculations agree with the UARS measurements within the range of their uncertainties.

Plate 3 shows a comparison between UARS measurements of ClO, $O_3$, $ClONO_2$, $HNO_3$, and SAD (inferred from extinction at 780 $cm^{-1}$) and model calculations using the fit scenarios for all parcels. Results for the 465, 520, and 585 K levels are shown by the green, red,

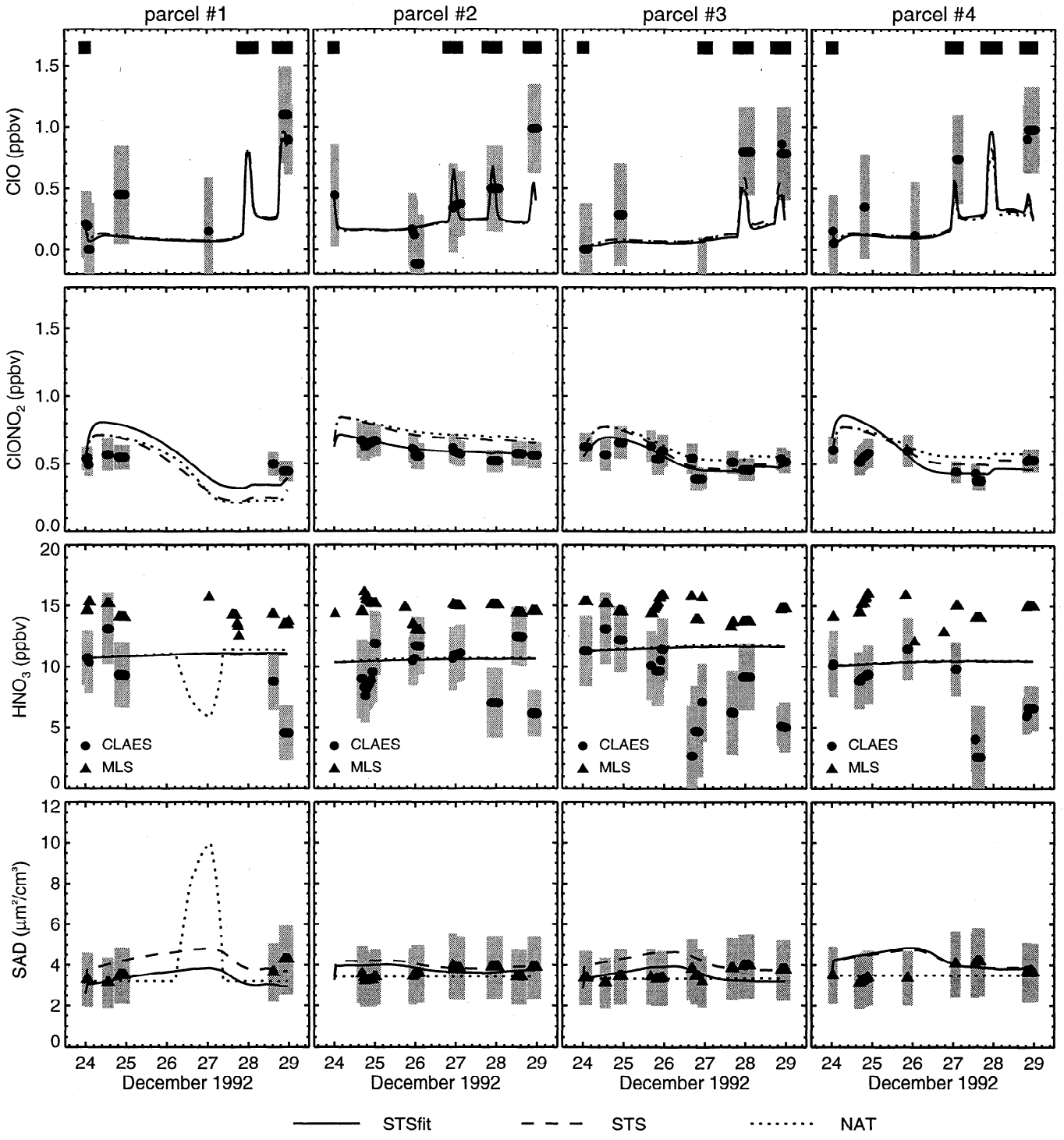


**Figure 1.** Evolution of ClO, $ClONO_2$, $HNO_3$ (all in ppbv), and SAD (in $\mu m^2/cm^3$) along the trajectories for parcels 1, 2, 3, and 4 ending at 465 K on December 29. The UARS measurements are shown by solid circles with grey error bars. Black bars near the top of the ClO panel indicate sunlit conditions (see Plate 2). Additionally, MLS v.5 $HNO_3$ are shown by solid triangles. Model calculations are shown by lines: dashed and dotted lines correspond to the baseline initialization for the STS and NAT schemes, respectively; solid lines correspond to the fit scenario with STS scheme (see text).

and blue symbols, respectively. Only one mean value for each matched clump of UARS data is shown, with the associated model value corresponding to the time of this mean UARS cluster value.

Previous model calculations systematically underestimated the simultaneous MLS ClO and CLAES $ClONO_2$ measurements at 465 K [e.g., *Chipperfield et al.*, 1996; *Lutman et al.*, 1997]. *Chipperfield et al.* [1996] even

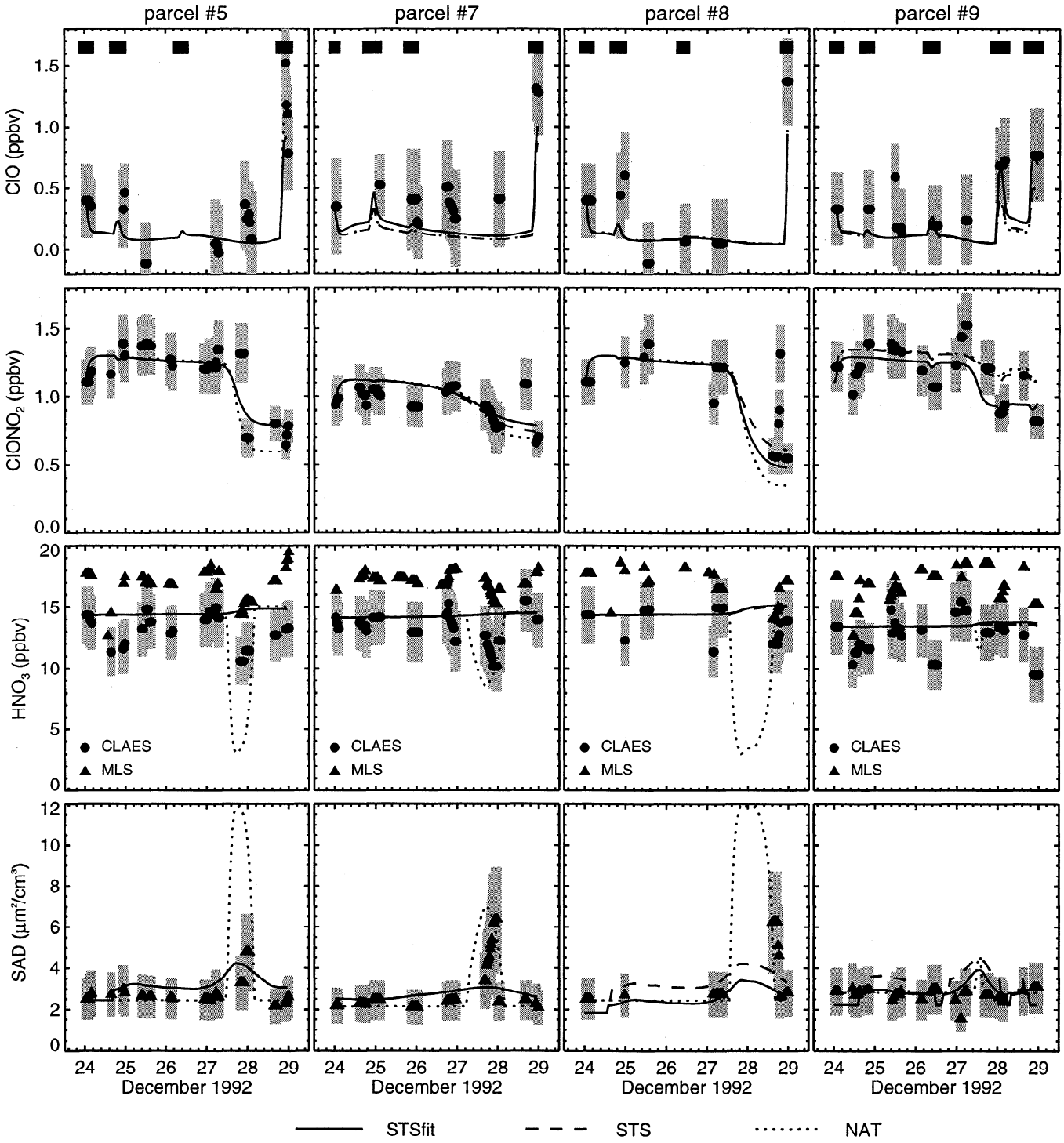


**Figure 2.** The same as in Figure 1, but for parcels 5, 7, 8, and 9 ending at 520 K on December 29.

speculated that MLS v.3 ClO and CLAES v.7 $ClONO_2$ could be inconsistent in some points. To check whether the final versions of MLS v.5 ClO and CLAES v.9 $ClONO_2$ are self-consistent for the chosen parcels, we perform stoichiometric calculations. These calculations are free from the possible model drawbacks and based on the following assumptions: (1) the $ClONO_2$ + HCl $\rightarrow$ $Cl_2$ + $HNO_3$ reaction is a principal mechanism of chlorine activation; (2) initial HCl > initial $ClONO_2$; (3) initial $Cl_2$ and $Cl_2O_2$ are small; and (4) all active chlorine is in ClO at the final point. The first assumption is very reasonable, bearing in mind the temperature history along the trajectories and the temperature dependence of the $ClONO_2$ + $H_2O$ and HOCl + HCl reactions [*DeMore et al.*, 1997]. The second assumption is consistent with the CLAES measurements

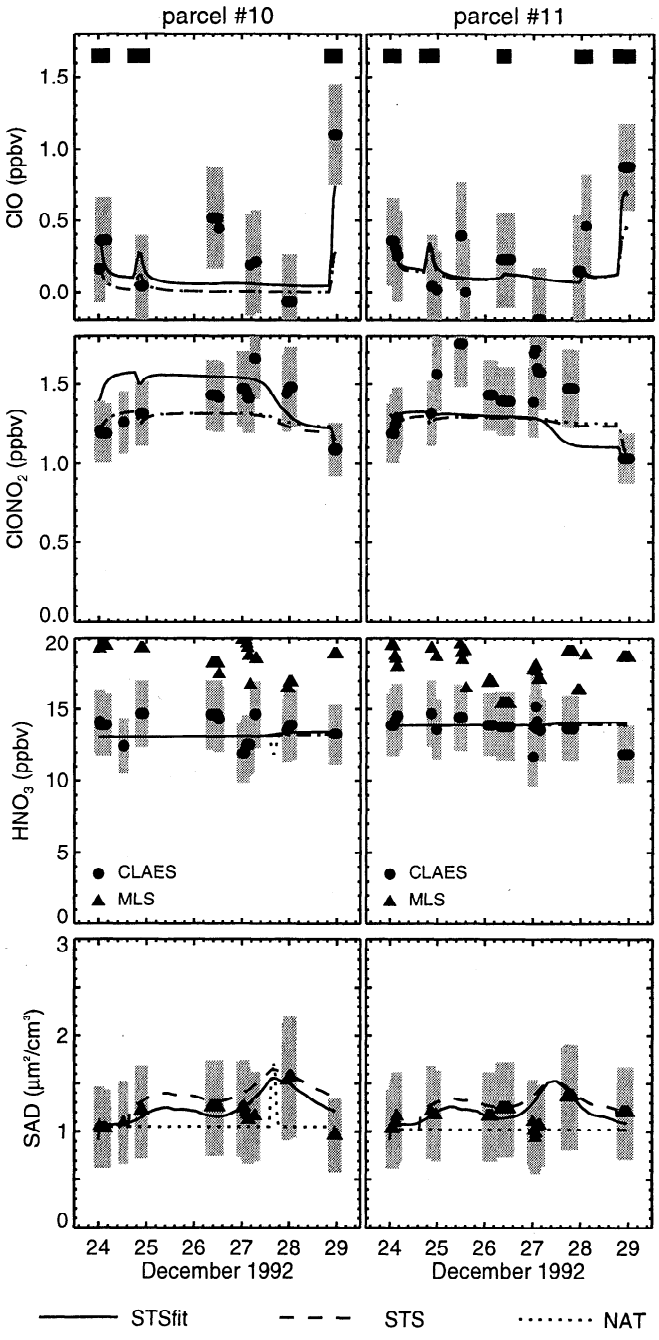


**Figure 3.** The same as in Figure 1, but for parcels 10 and 11 ending at 585 K on December 29.

for the episode studied. The third assumption is supported by the warm temperature along the backward trajectories and the ClO and $ClONO_2$ measurements 10 days prior to December 24, 1992, suggesting that conversion of HCl and $ClONO_2$ to other active chlorine forms ($Cl_2O_2$ and $Cl_2$), undetectable by MLS, is unlikely. The fourth assumption is too strong for the final points with SZA of 85°-90°, but it provides an upper bound for ClO. On the basis of these assumptions the maximum increase in chlorine monoxide, $\Delta ClO^{max}$, equals $2ClONO_2^{ini} - ClONO_2^{fin}$. This expression shows that if all initial $ClONO_2^{ini}$ is consumed via the $ClONO_2 + HCl \longrightarrow Cl_2 + HNO_3$ reaction, then the $Cl_2$ produced could photolyze, producing two ClO molecules per one $Cl_2$ molecule. From these ClO molecules the fraction equal to $ClONO_2^{fin}$ could be lost via the $ClO + NO_2 + M \longrightarrow ClONO_2 + M$ reaction. Since the amount of $ClONO_2$ is a limiting factor of chlorine activation, to obtain the maximum possible increase in ClO one can assume that the initial $ClONO_2$ equals $ClONO_2^{ini}+1\sigma$ and the final $ClONO_2$ equals $ClONO_2^{fin}-1\sigma$. Taking into account that $\sigma$ is equal to 20% for the individual CLAES v.9 $ClONO_2$ measurements, the maximum ClO increase is calculated according to

$$\Delta ClO^{MAX} = 2.4ClONO_2^{ini} - 0.8ClONO_2^{fin}. \quad (2)$$

Our stoichiometric calculations show that for all 11 parcels MLS v.5 ClO and CLAES v.9 $ClONO_2$ are self-consistent within the range of their individual measurement uncertainties.

Our model calculations (as seen in Figures 1-3 and Plate 3) also tend to underpredict the ClO concentration at 465 K; however, they usually agree with MLS v.5 ClO measurements within the range of their error bars. We attribute the better agreement between the modeled and measured ClO to the better constrained model calculations and the use of MLS v.5 retrieval algorithms, which resulted in reduced ClO values in the lower stratosphere compared with previous v.4 data [*N. Livesey et al., manuscript in preparation*]. However, more extensive modeling studies are required to justify this conclusion under all atmospheric conditions.

The rapid increase in ClO in Figures 1-3 can be attributed not only to chlorine activation but also to sunlit conditions. To illustrate the effect of the presence of

**Table 2.** Details of the Model Initializations and Temperature Along the Trajectories for the Fit Scenarios With the STS Scheme

| Parcel | Changes From the Baseline Case |
|---|---|
| 1 | SAD down by 20% |
| 2 | $NO_x$ = 0.1 ppbv |
| 3 | SAD down by 15% and $ClONO_2$ down by 10% |
| 4 | $ClONO_2$ up by 15% and temperature lowered by 1 K |
| 5 | no changes |
| 6 | SAD down by 20% |
| 7 | $NO_x$ = 0.3 ppbv |
| 8 | SAD down by 20% and temperature lowered by 1 K |
| 9 | SAD down by 20%, $ClONO_2$ down by 10%, and temperature lowered by 2 K |
| 10 | SAD down by 10%, $ClONO_2$ up by 15%, and temperature lowered by 2 K |
| 11 | SAD down by 10% and temperature lowered by 2 K |

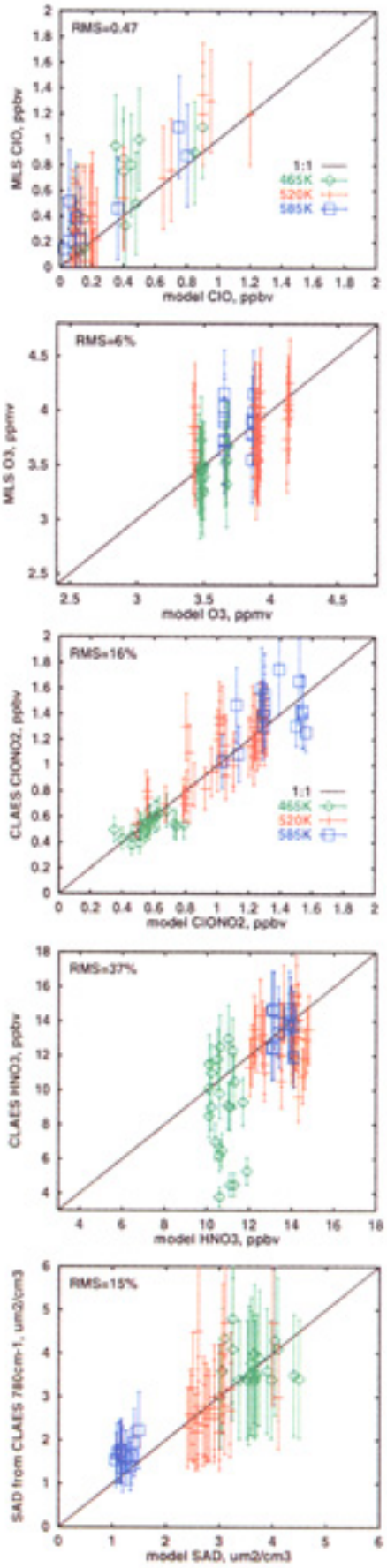


sunlight, we indicate the intervals when the parcels were illuminated by horizontal black bars in the ClO panels. This information also could be obtained from Plate 2 when the SZA along the trajectories is smaller than the values shown by the horizontal line. On the other hand, a rapid reduction in $ClONO_2$ signals chlorine activation. The magnitude of the anticipated change in ClO due to chlorine activation can be estimated as twice the value of the $ClONO_2$ reduction. For example, the first large spike in ClO for parcels 4 and 9 is attributed to both chlorine activation and sunlit conditions, while the second spike is due to the presence of sunlight only (since $ClONO_2$ remains practically unchanged).

Our results in Figures 1-3 also show that liquid ambient aerosol can activate chlorine efficiently even at temperatures above the NAT threshold. Similar conclusions were reached based on observations made during the ASHOE/MAESA aircraft campaign in 1994 by *Kawa et al.* [1997] and based on model calculations by *Michelsen et al.* [1999]. UARS MLS measurements and our model calculations for this episode in December 1992 show that a rapid increase in ClO up to 1-1.2 ppbv in the lower stratosphere can be obtained without a simultaneous decrease in $HNO_3$ and a considerable increase in aerosol extinction (i.e., SAD), which are indicators of PSC events. Thus cold temperature (below 200 K) is a necessary condition for chlorine activation, while an exponential increase in heterogeneous reaction rates with decreasing temperature is a principal mechanism facilitating conversion of HCl and $ClONO_2$ to $ClO_x$.

The important conclusion we draw from the above analysis is that MLS v.5 ClO and CLAES v.9 $ClONO_2$ are consistent with each other and agree with the model calculations within their uncertainties for the episode considered. Use of equation (1) by *Massie et al.* [1998] allows us to convert CLAES extinctions at 780 $cm^{-1}$ to SAD, and our model calculations show an excellent agreement with CLAES data for all parcels in the lower stratosphere. When coefficients for the 3-6% $HNO_3$ ternary solutions are used from *Massie et al.* [1998, Tables 4-6], the SAD values are reduced by 5-10% for the parcels considered. However, these changes exist only during short periods of time when temperature is cold enough for STS formation, and thus do not af-

**Plate 3.** Comparison of MLS v.5 ClO and CLAES v.9 $ClONO_2$, $HNO_3$, and SAD (converted from the 780 $cm^{-1}$ extinction) measurements with AER model calculations along all trajectories from the fit scenarios at 465 (green), 520 (red), and 585 K (blue). Initial points on December 24 are excluded from this comparison. Details of the fit scenarios are given in the text. Root-mean-square (RMS) values are shown in percent.

fect strongly the shown agreement between the model calculations and CLAES 780 $cm^{-1}$ measurements. A similar conclusion is likely for the NAT case. Also, our study does not support concerns mentioned by *Hervig and Deshler* [1998] that CLAES measurements overestimate the aerosol extinction under Antarctic conditions. The reason is that for the relatively benign conditions of the Arctic vortex (i.e., warmer temperatures and thinner PSCs) the CLAES extinction measurements do not degrade to the extent reported by *Hervig and Deshler* [1998] for Antarctic winter vortex.

The individual CLAES v.9 and MLS v.5 $HNO_3$ measurements are more scattered (especially at lower levels) but show usually similar behavior along the trajectories. However, as discussed in section 2.1, the MLS v.5 $HNO_3$ is systematically higher than the CLAES v.9 $HNO_3$. In addition, the CLAES data exhibit more variability along the trajectories than is evident in either the MLS data or the model simulations. This discrepancy most likely arises from a number of sources. In comparison to correlative data, CLAES v.7 retrievals underestimated $HNO_3$ abundances when peak mixing ratios were less than 8 ppbv but overestimated them when peak mixing ratios were greater than 8 ppbv [*Kumer et al.*, 1996]. Although a sufficient number of comparisons with correlative data sets have not yet been made to ascertain whether this remains true for v.9 $HNO_3$ data, this effect could magnify the apparent variability in the CLAES measurements. Another contributing factor could be differences in the air parcels being sampled. Running the model along individual trajectories ensures that the behavior of the same air parcels is followed throughout the entire simulation, and the model results are therefore quite smooth. Although we have taken considerable care to examine measurements of the same parcels as those represented in the model simulations, small errors in colocation could lead to differences between model and observation and variations in the measured quantity from one point to another along the trajectory. In addition, since CLAES has a smaller horizontal footprint in the direction perpendicular to the line of sight than does MLS, the two instruments do not sample the exact same parcel of air, and CLAES is likely to be more sensitive than MLS to small-scale inhomogeneities in the $HNO_3$ field.

A sensitivity study using MLS v.5 $HNO_3$ to initialize the model calculations (not shown) produced results similar to those in Figures 1-3. The reason for the relatively weak sensitivity of the model results to the choice of initial $HNO_3$ lies with the fact that the higher MLS $HNO_3$ abundances (usually by 2-3 ppbv compared with CLAES $HNO_3$) can be translated into larger SAD at T<200 K. However, the same ClO and $ClONO_2$ in the final points could be obtained using slightly reduced initial SAD when MLS $HNO_3$ is used for the model initialization. Thus the relatively large uncertainties in the individual UARS measurements preclude us from determining which instrument (CLAES or MLS) provides "correct" $HNO_3$ measurements. However, reconciliation of the CLAES and MLS $HNO_3$ measurements is important from the standpoint of global models, which cover multimonth periods and perform ozone calculations that are sensitive to $HNO_3$ and SAD.

To quantify the agreement between model calculations and UARS measurements, we calculated root-mean-square (RMS) values for each species (shown in the left top corner of each panel in Plate 3). The worst agreement between model and measurements are obtained for $HNO_3$ (RMS=37%) and ClO (RMS=47%), while for $O_3$ (RMS=6%), $ClONO_2$ (RMS=16%), and SAD (RMS=15%), model results are closer to the measurements.

The uncertainties of the UKMO analyzed temperatures and the error bars of the individual UARS measurements used in this study are too large to make a robust conclusion about which PSC scheme better describes the measurements in this episode. For example, for all parcels at the 465 and 585 K levels both PSC schemes produce very similar results for ClO, $ClONO_2$, $HNO_3$, and SAD that are consistent with the measurements within their error bars. Thus the ClO and $ClONO_2$ data do not allow us to discriminate between different PSC schemes at 520 K. Analyzing aircraft measurements, *Kawa et al.* [1997] also noted that it is difficult to distinguish different PSC schemes based on chlorine species measurements because: (1) the PSC reactions make similar changes in stratospheric composition (albeit with different rates) and (2) measurement uncertainties are large. Results for $HNO_3$ and SAD at 520 K shown for parcels 5, 7, and 8 in Figure 2 look more supportive for the NAT scheme. This statement is supported by MLS and CLAES instruments, both showing a few ppbv reduction of $HNO_3$ along these trajectories on December 28. However, the details of PSC formation could not be resolved for this episode due to uncertainties of the UKMO temperature. For example, we obtained a better agreement between model and CLAES measurements of $HNO_3$ and SAD when a supersaturation of three is applied in our NAT scheme. On the other hand, practically the same results are obtained for a supersaturation of 10 and UKMO temperature lowered by 2 K. Thus a larger set of statistics is required to deduce how PSCs are formed, using approaches similar to those of *Santee et al.* [1998] and *Dessler et al.* [1999].

As an additional sensitivity analysis, we applied the trajectory hunting technique for this episode of chlorine activation using isentropic trajectories. Our model results along isentropic trajectories (not shown here) are very similar to those shown in Figures 1-3 for the diabatic trajectories. This could be anticipated since the difference between diabatic and isentropic trajectories is rather small. For instance, diabatic effects lead to a

difference of about 200-300 m vertically for initial points on December 24 and typically less than 1° in latitude and a few degrees in longitude. Thus our conclusions in this paper are not sensitive to accounting for diabatic effects for the trajectory calculations. However, for longer runs (10 days or more) diabatic effects could become more important due to longer accumulation time.

We also investigated the effects of the MLS ClO uncertainties on the initial $Cl_2O_2$ and the conclusions of our study. Initial $Cl_2O_2$ is very sensitive to the SZA since its photolysis is fast ($J_{Cl2O2}>10^{-4}$ $s^{-1}$ at SZA<89° above 20 km). Thus initial $Cl_2O_2$ is not sensitive to uncertainties in the initial ClO at sunlit starting points of the parcels 5, 8, 9, 10, and 11. For the other parcels, use of $ClO^{ini} + 1\sigma$ produces larger $Cl_2O_2^{ini}$ and facilitates obtaining high ClO at the final points of these trajectories. The higher final ClO values are obtained at the expense of HCl in this case, and thus they do not affect our model agreement with the CLAES $ClONO_2$, $HNO_3$, and SAD measurements. Only limited reduction of $Cl_2O_2^{ini}$ is obtained when $ClO^{ini}$ - $1\sigma$ is used, since only small $ClO^{ini}$ is chosen for this study. The model ClO results are reduced for parcel 2 only. However, even in this worst case, model and MLS ClO values agree within their uncertainties at all intermediate points. Thus, large uncertainties in initial ClO values do not affect the conclusions of this study.

We also performed a visual analysis of daily maps of the MLS ClO and CLAES aerosol 780 $cm^{-1}$ measurements during two northlooking UARS yaw cycles from December 1992 to March 1993 at 465, 520, and 585 K. We did not find any situations in which high aerosol extinctions were not accompanied by elevated levels of ClO, thus supporting the existing concept of chlorine activation via heterogeneous reactions.

To test the validity of our approach for regions in which the chlorine had not been activated, we applied this technique to analyze CLAES and MLS data for the same days but for points with relatively low ClO values (less than 0.25 ppbv on December 29). For six parcels satisfying our match criteria at 465, 520, and 585 K, we saw less scattered MLS and CLAES data than those in Figures 1-3. Also, a good agreement between model calculations and measurements is obtained (not shown here) even for the baseline initialization of the model (i.e., the fit scenarios could provide near-perfect agreement for these parcels). This test is encouraging showing potentially wide (i.e., not limited to a particular event or process) applications of the trajectory hunting technique.

Our analysis of UARS data indicating rapid chlorine activation is only one of the possible applications of the trajectory hunting technique. This technique can help, for example, to merge measurements of different platforms (satellites, aircraft, balloons, lidars, radars, etc.). In this case, data from the different platforms can complement each other, thus creating extended data sets and providing better constraints for subsequent model analyses. The spatial and temporal coverage of such data sets can also be expanded. The trajectory hunting technique could be particularly useful for an intensive validation study of a new instrument or platform.

## 6. Summary

We presented results of an application of the trajectory hunting technique for an episode of rapid chlorine activation in the stratosphere in December 1992. In this case study, the trajectory hunting technique allows us to find air parcels sampled several times by UARS from December 24 to 29, 1992, and to investigate the evolution of photochemically active species and aerosol along these parcel trajectories. This approach reduces the dynamical effects from our analysis and puts sophisticated constraints on the model calculations, thus allowing comparison of the model representation of stratospheric chemistry with individual UARS measurements. Our analysis shows that for the December 24-29, 1992, episodes (1) the model usually agrees with MLS v.5 ClO measurements within the range of their uncertainties; however, the model still tends to underpredict the ClO content, especially at 465 K; (2) the model shows good agreement with CLAES v.9 $ClONO_2$ and aerosol extinction at 780 $cm^{-1}$ (converted to SAD using equation (1)) at all three levels (585, 520, and 465 K); (3) in general, model results agree with the CLAES v.9 $HNO_3$ data within the range of their uncertainties; however, at 465 K this agreement is relatively poor; (4) the individual MLS v.5 ClO and CLAES v.9 $ClONO_2$ and 780 $cm^{-1}$ extinction measurements are self-consistent; and (5) the UARS measurements for this episode could be explained by either NAT or STS PSC schemes; for parcels 5-8 at 520 K the UARS measurements look more supportive for the NAT scheme; overall a larger set of statistics is required to distinguish between these schemes.

Thus our major conclusions drawn from this study of a chlorine activation episode in December 1992 are (1) CLAES v.9 $ClONO_2$ and MLS v.5 ClO measurements show a consistent picture; and (2) the model representation of the PSC processes is supported by the UARS measurements. These conclusions are based on the episode considered, and a more detailed study is required to check the validity of these statements for the whole CLAES and MLS data sets.

**Acknowledgments.** We thank G. L. Manney for the use of her trajectory model and the UKMO for meteorological data. We appreciate the MLS $H_2O$ values provided by H. C. Pumphrey. Discussions with S. T. Massie regarding conversion of CLAES extinction measurements to surface area density are appreciated. We thank reviewers for their comments. Work at the Jet Propulsion Laboratory, California Institute of Technology, was done under contract with NASA. Work at AER, Inc. was supported by the UARS Guest Investigator Program (NAS5-32844 and NAS5-98131) and NASA ACMAP (NAS5-97039).

## References


Bacmeister, J.T., et al., Intercomparison of satellite and aircraft observations of $O_3$, CFC-11, and $NO_y$ using trajectory mapping, *J. Geophys. Res., 104*, 16,379-16,390, 1999.

Barath, F.T., et al., The Upper Atmosphere Research Satellite Microwave Limb Sounder instrument, *J. Geophys. Res., 98*, 10,751-10,762, 1993.

Chipperfield, M.P., et al., Analysis of UARS data in the southern polar vortex in September 1992 using a chemical transport model, *J. Geophys. Res., 101*, 18,861-18,881, 1996.

Danilin, M.Y., N.D. Sze, M.K.W. Ko, J.M. Rodriguez, and A. Tabazadeh, Stratospheric cooling and Arctic ozone recovery, *Geophys. Res. Lett., 25*, 2141-2144, 1998.

DeMore, W.B., et al., Chemical kinetics and photochemical data for use in stratospheric modeling, *JPL Publ. 97-4*, 1997.

Dessler, A.E., J. Wu, M.L. Santee, and M.R. Schoeberl, Satellite observations of temporary and irreversible denitrification, *J. Geophys. Res., 104*, 13,993-14,002, 1999.

Hanson, D.R., and K. Mauersberger, Laboratory studies of nitric acid trihydrate: Implications for the south polar stratosphere, *Geophys. Res. Lett., 15*, 855-858, 1988.

Hervig, M.E., and T. Deshler, Stratospheric aerosol surface area and volume inferred from HALOE, CLAES, and ILAS measurements, *J. Geophys. Res., 103*, 25,345-25,352, 1998.

Kawa, S.R., et al., Photochemical partitioning of the reactive nitrogen and chlorine reservoirs in the high-latitude stratosphere, *J. Geophys. Res., 97*, 7905-7923, 1992.

Kawa, S.R., et al., Activation of chlorine in sulfate aerosol as inferred from aircraft observations, *J. Geophys. Res., 102*, 3921-3934, 1997.

Kumer, J.B., Comparison of correlative data with $HNO_3$ version 7 from the CLEAS instrument deployed on the NASA UARS, *J. Geophys. Res., 101*, 9621-9656, 1996.

Knudsen, B.M., Accuracy of Arctic stratospheric temperature analysis and the implications for the prediction of polar stratospheric clouds, *Geophys. Res. Lett., 23*, 3747-3750, 1996.

Lutman, E.R., et al., Three-dimensional studies of the 1991/1992 northern hemisphere winter using domain-filling trajectories with chemistry, *J. Geophys. Res., 102*, 1479-1488, 1997.

Manney, G.L., et al., On the motion of air through the stratospheric polar vortex, *J. Atmos. Sci., 51*, 2973-2994, 1994.

Manney, G.L., et al., Lagrangian transport calculations using UARS data: I. Passive tracers, *J. Atmos. Sci., 52*, 3049-3068, 1995.

Manney, G.L., et al., Arctic ozone depletion observed by UARS MLS during the 1994-1995 winter, *Geophys. Res. Lett., 23*, 85-88, 1996a.

Manney, G.L., et al., Comparison of U.K. Meteorological Office and U.S. National Meteorological Center stratospheric analyses during northern and southern winter, *J. Geophys. Res., 101*, 10,311-10,334, 1996b.

Massie, S.T., et al., Validation studies using multiwavelength CLAES observations of stratospheric aerosol, *J. Geophys. Res., 101*, 9757-9773, 1996.

Massie, S.T., et al., Estimation of PSC volume and area densities from UARS, SAM II, and POAM II extinction data, *J. Geophys. Res., 103*, 5773-5783, 1998.

Mergenthaler, J.L., et al., Validation of CLAES $ClONO_2$ measurements, *J. Geophys. Res., 101*, 9603-9620, 1996.

Michelsen, H.A., C.M.Spivakovsky, and S.C. Wofsy, Aerosol-mediated partitioning of stratospheric $Cl_y$ and $NO_y$ at temperatures above 200 K, *Geophys. Res. Lett., 26*, 299-302, 1999.

Morris, G.A., et al., Trajectory mapping and applications to data from the Upper Atmosphere Research Satellite, *J. Geophys. Res., 100*, 16,491-16,505, 1995.

Pierce, R.B., et al., Photochemical calculations along air mass trajectories during ASHOE/MAESA, *J. Geophys. Res., 102*, 13,153-13,168, 1997.

Pumprey, H.C., Validation of a new prototype water vapor retrieval for UARS MLS, *J. Geophys. Res., 104*, 9399-9412, 1999.

Rex, M., et al., Prolonged stratospheric ozone loss in the 1995-96 Arctic winter, *Nature, 389*, 835-838, 1997.

Rex, M., et al., In situ measurements of stratospheric ozone depletion rates in the Arctic winter 91/92: A Lagrangian approach, *J. Geophys. Res., 103*, 5843-5853, 1998.

Roche, A.E., et al., The cryogenic limb array etalon spectrometer (CLAES) on UARS: Experiment description and performance, *J. Geophys. Res., 98*, 10,763-10,775, 1993.

Roche, A.E., et al., Validation of $CH_4$ and $N_2O$ measurements by CLAES on UARS, *J. Geophys. Res., 101*, 9679-9710, 1996.

Santee, M.L., G.L. Manney, W.G. Read, L. Froidevaux, and J.W. Waters, Polar vortex conditions during the 1995-1996 Arctic winter: MLS ClO and $HNO_3$, *Geophys. Res. Lett., 23*, 3207-3210, 1996.

Santee, M.L., G.L. Manney, L. Froidevaux, R.W. Zurek, and J.W. Waters, MLS observations of ClO and $HNO_3$ in the 1996-1997 Arctic polar vortex, *Geophys. Res. Lett., 24*, 2713-2716, 1997.

Santee, M.L., et al., UARS MLS $HNO_3$ observations: Implications for Antarctic PSCs, *J. Geophys. Res., 103*, 13,285-13,313, 1998.

Santee, M.L., et al., Six years of UARS MLS $HNO_3$ observations: Seasonal, interhemispheric, and interannual variations in the lower stratosphere, *J. Geophys. Res., 104*, 8225-8246, 1999.

Schoeberl, M.R., and L.C. Sparling, Trajectory modelling, in *Diagnostic Tools in Atmospheric Physics, Proc. International School of Physics, Enrico Fermi, Course CXVI*, eds. G. Fiocco and G. Visconti, pp. 289-305, North-Holland, New York, 1995.

Shine, K.P., The middle atmosphere in the absence of dynamic heat fluxes, *Q. J. R. Meteorol. Soc., 113*, 603-633, 1987.

Steele, H.M., K. Drdla, R.P. Turco, J.D. Lumpe, and R.M. Bevilacqua, Tracking polar stratospheric cloud development with POAM II and microphysical model, *J. Geophys. Res., 26*, 287-290, 1999.

Swinbank, R., and A. O'Neill, A stratosphere-troposphere data assimilation system, *Mon. Weather Rev., 122*, 686-702, 1994.

Tabazadeh, A., et al., A model for studying the composition and chemical effects of stratospheric aerosol, *J. Geophys. Res., 99*, 12,897-12,908, 1994.

von der Gathen, P., et al., Observational evidence for chemical ozone depletion over the Arctic in winter 1991-92, *Nature, 375*, 131-134, 1995.

Wamsley, P.R., et al., Distribution of halon-1211 in the upper troposphere and lower stratosphere and the 1994 total bromine budget, *J. Geophys. Res., 103*, 1513-1526, 1998.

Waters, J.W., Microwave limb sounding, in *Atmospheric Remote Sensing by Microwave Radiometry*, edited by M. A. Janssen, pp. 383-496, John Wiley, New York, 1993.

Waters, J.W., et al., Stratospheric ClO and ozone from the Microwave Limb Sounder on the Upper Atmosphere Research Satellite, *Nature, 362*, 597-602, 1993.

Waters, J.W., et al., UARS MLS observations of lower

stratospheric ClO in the 1992-93 and 1993-94 Arctic winter vortices, *Geophys. Res. Lett., 22*, 823-826, 1995.

Waters, J.W., et al., Validation of UARS microwave limb sounder ClO measurements, *J. Geophys. Res.,101*, 10,091-10,127, 1996.

Woodbridge, E.L., et al., Estimates of total organic and inorganic chlorine in the lower stratosphere from in situ and flask measurements during AASE II, *J. Geophys. Res., 100*, 3057-3064, 1995.

M. Y. Danilin and M. K. W. Ko, AER, Inc., 840 Memorial Drive, Cambridge, MA 02139. (danilin@aer.com)

J. B. Kumer and J. L. Mergenthaler, Lockheed Martin Advanced Technology Center, 3251 Hanover Street, Palo Alto, CA 94304-1191.

N. J. Livesey and M. L. Santee, NASA JPL, Mail Stop 183-701, 4800 Oak Grove Drive, Pasadena, CA 91109.

J. M. Rodriguez, Department of Marine and Atmospheric Chemistry, University of Miami, 4600 Rickenbacker Causeway, Miami, FL 33149.

A. Tabazadeh, NASA Ames Research Center, Mail Stop 245-4, Moffett Field, CA 94035.

(Received May 19, 1999; revised October 8, 1999; accepted October 13, 1999.)